2020 EAGE ANNUAL
82ND CONFERENCE + EXHIBITION
AMSTERDAM | THE NETHERLANDS
NOW IN WINTER
8-11 DECEMBER

We_Dome5_15

High-Resolution Angle Gathers from Iterative Least-Squares Migration

L. Duan[1]*, D. Whitmore[1], N. Chemingui[1], E. Klochikhina[1]

[1] PGS

Summary

Using wave-equation migration and demigration in the extended subsurface domain, we introduce a practical least-squares migration for the inversion of angle-domain common-image gathers. Through synthetic and field data examples, we demonstrate that least-squares migration provides high-resolution angle-domain common-image gathers with extended angle range, enhanced illumination, and balanced amplitudes. Similarly, the stacked images show better structural fidelity, improved resolution, balanced illumination, and reduced artifacts.

Introduction

Depth migration often yields an image with insufficient illumination and resolution that can be attributed to acquisition limitations. To resolve the problem, the framework of Least-Squares Migration (LSM), seeks an inverted reflectivity image which minimizes a difference metric between the modeled and recorded data. It has recently been made possible to use LSM for daily practice and production. However, a practical and stable formulation of LSM in the prestack domain still remains a challenge.

In this work, we describe a general framework of prestack LSM. We derive the numerical solution of LSM in the extended subsurface domain and formulate its conjugate gradient inversion scheme with a split Bregman step to regularize the model sparsity. Compared to a conventional migration solution, applications to both synthetic and field data demonstrate that the proposed LSM can produce high-resolution Angle-Domain Common-Image Gathers with enhanced angle range, improved illumination, and balanced amplitudes and results in stacked images with better structural fidelity, improved resolution, balanced illumination, and reduced artifacts.

Theory

We consider seismic data $D(\boldsymbol{x_r};\boldsymbol{x_s};\omega)$ in angular frequency ω with the shot at $\boldsymbol{x_s}=(x_s,y_s,z_s=0)$ and receiver at $\boldsymbol{x_r}=(x_r,y_r,z_r=0)$ and assume regular surface sampling and infinite recording aperture. Wave-equation migration (WEM) is able to provide a true-amplitude angle-dependent reflectivity image by the downward extrapolation of the source wavefield P_D with the designatured zero phase source wavelet $f(\omega)$ (Valenciano et al., 2011):

$$\begin{cases} (\partial_z + \mathrm{i}\Lambda)P_D(\boldsymbol{x};\boldsymbol{x_s};\omega)=0, \\ P_D(\boldsymbol{x},0;\boldsymbol{x_s},0;\omega)=\delta(\boldsymbol{x}-\boldsymbol{x_s})f(\omega), \end{cases} \tag{1}$$

and the upgoing extrapolation of the receiver wavefield P_U:

$$\begin{cases} (\partial_z - \mathrm{i}\Lambda)P_U(\boldsymbol{x};\boldsymbol{x_s};\omega)=0, \\ P_U(\boldsymbol{x},0;\boldsymbol{x_s},0;\omega)=D(\boldsymbol{x_r};\boldsymbol{x_s};\omega), \end{cases} \tag{2}$$

We extend the imaging condition with a directional space shift at the subsurface locations $\boldsymbol{x}=(x,y,z)$ to create prestack subsurface offset domain common image gather (ODCIG) $r(\boldsymbol{x},\boldsymbol{h})$:

$$r(\boldsymbol{x},\boldsymbol{h})=\iint \frac{P_U(\boldsymbol{x}+\boldsymbol{h};\boldsymbol{x_s};\omega)P_D^H(\boldsymbol{x}-\boldsymbol{h};\boldsymbol{x_s};\omega)}{\langle P_D(\boldsymbol{x}-\boldsymbol{h};\boldsymbol{x_s};\omega)P_D^H(\boldsymbol{x}+\boldsymbol{h};\boldsymbol{x_s};\omega)\rangle_{\boldsymbol{x}}+\epsilon(\boldsymbol{x};\boldsymbol{x_s};\omega)}\,d\omega\,d\boldsymbol{x_s}. \tag{3}$$

Here, ∂_z denotes the partial derivative respect to z; Λ is the extrapolation operator; $\boldsymbol{h}=(h_x,h_y)$ denotes the source-receiver half offset; $\langle\,\rangle_{\boldsymbol{x}}$ denotes the preconditioning of the downgoing wavefield subject to its subsurface location $\boldsymbol{x}$, and ϵ is a stabilization term for the subsurface locations with poor signal energy. For Angle Domain Common Image Gathers (ADCIG), the ODCIG in (3) can be transformed through a radial-trace transformation (Fomel, 2011).

The image using this migration process can have imperfections due to acquisition and because equations (1-3) are the adjoint of modeling the reflectivity:

$$r(\boldsymbol{x},\boldsymbol{h})=M^T d(\boldsymbol{x_r};\boldsymbol{x_s};\omega), \tag{4}$$

where M denotes the (Born) modeling operator. Ideally we want an inverse to this operator. Least-squares migration (LSM) attempts to achieve this by minimizing a cost function $\mathrm{E}(r)$ combining the total data matching between the recorded data $D(\boldsymbol{x_r};\boldsymbol{x_s};\omega)$ and the modeled data $d(\boldsymbol{x_r};\boldsymbol{x_s};\omega)$ and a sparsity promotion using L_1 total variation regularization (TVR) as follows:

$$\mathrm{E}(r)=\frac{1}{2}\iiint (D-d)^2\,d\boldsymbol{x_r}d\boldsymbol{x_s}d\omega+\iiint \left(|\lambda_x\partial_x r|+|\lambda_y\partial_y r|+|\lambda_z\partial_z r|\right)dx\,dy\,dz\,dh_x\,dh_y. \tag{5}$$

Here, λ_x, λ_y and λ_z are the regularization scalars for the reflectivity variation to ensure the inversion stability such as non-physical migration swings and better sparsity in the inverted image, and $d=M(r)$ is generated by a Born demigration process adjoint to WEM in equations (1-3):

$$\begin{cases} (\partial_z + \mathrm{i}\Lambda)P_D(\boldsymbol{x};\boldsymbol{x_s};\omega)=\delta(\boldsymbol{x}-\boldsymbol{x_s})f(\omega), \\ (\partial_z - \mathrm{i}\Lambda)P_U(\boldsymbol{x};\boldsymbol{x_s};\omega)=-\omega^2\sum_{\boldsymbol{h}} r(\boldsymbol{x},\boldsymbol{h})\,P_D(\boldsymbol{x}+\boldsymbol{h};\boldsymbol{x_s};\omega), \\ d(\boldsymbol{x_r};\boldsymbol{x_s};\omega)=P_U(\boldsymbol{x_r};\boldsymbol{x_s};\omega). \end{cases} \tag{6}$$

To establish a stable and efficient inversion scheme, we write the numerical solution of the LSM in equation (5) in an equivalent form with weakly enforced constraints (Qiu et al., 2016):

$$\min_{r,q}\left[\frac{1}{2}\iiint (D-M(r))^2\, d\boldsymbol{x_r}\, d\boldsymbol{x_s}\, d\omega + \frac{\gamma_l}{2}\iint (r-l)^2\, d\boldsymbol{x}\, d\boldsymbol{h} + \frac{\gamma_q}{2}\iint (q-\nabla l-b)^2\, d\boldsymbol{x}\, d\boldsymbol{h} + \iiint \left(|\lambda_x q_x| + |\lambda_y q_y| + |\lambda_z q_z|\right) dx\, dy\, dz\, dh_x\, dh_y\right]. \quad (7)$$

Here, ∇ denotes the vector derivative; γ_l and l are the weakly constrained Lagrange multiplier and variable for the reflectivity r, respectively; γ_q and $q=(q_x,q_y,q_z)$ are the weakly constrained Lagrange multiplier and variable related to the total variation constraint, respectively; and b is the auxiliary variable. Using the split Bregman algorithm, the numerical solution of equation (7) can be rewritten as an iterative update:

$$r_i = \arg\min_r \left[\frac{1}{2}\iiint \left(D-M(r)\right)^2 d\boldsymbol{x_r}\, d\boldsymbol{x_s}\, d\omega + \frac{\gamma_l}{2}\iint (r-l_{i-1})^2\; d\boldsymbol{x}\, d\boldsymbol{h}\right], \quad (8)$$

$$l_i = \arg\min_l \left[\frac{\gamma_l}{2}\iint (r_i-l)^2 d\boldsymbol{x}\, d\boldsymbol{h} + \frac{\gamma_q}{2}\iint (q_{i-1}-\nabla l-b_{i-1})^2\, d\boldsymbol{x}\, d\boldsymbol{h}\right], \quad (9)$$

$$q_i = \arg\min_q \left[\frac{\gamma_q}{2}\iint (q-\nabla l_i-b_{i-1})^2 d\boldsymbol{x} d\boldsymbol{h} + \iint \left(|\lambda_x q_x| + |\lambda_y q_y| + |\lambda_z q_z|\right) dx dy dz dh_x dh_y\right], \quad (10)$$

$$b_i = b_{i-1} + \nabla l_i - q_i. \quad (11)$$

The first suboptimal problem (8) is the standard LSM with a L_2 total variation with well-established numerical solutions (e.g. Lu et al., 2018). For the total variation constraints in suboptimal problems (9-11), we can rewrite it as a Least Absolute Shrinkage and Selection Operator (LASSO) problem and adapt it as a Shrinkage Thresholding Operator as in Duan et al., 2017.

Least-Squares Migration (LSWEM) Scheme

Given the recorded data D and source signature f, our LSWEM is summarized as follows:

1. Conduct reflectivity inversion. Initialize: $r_0 = M^T(D)$, $d_0 = M(r_0)$,
2. For $j = 1,2,3,\ldots$ repeat steps 4-8 and exit with $r = r_j$ if stopping criterion has been met:
3. Calculated the image domain steepest descent direction as $\delta r_j = M^T\left(D - d_{j-1}\right)$.
4. Compute Polak–Ribière conjugate gradient weighting $\beta_j = \max\left(0, \frac{\int \delta r_j(\delta r_j - \delta r_{j-1})dx}{\int \delta r_j \delta r_j dx}\right)$.
5. Update the conjugate gradient direction $\delta s_j = \delta r_j + \beta_j \delta s_{j-1}$.
6. Calculated the linear search for a scaler $\epsilon = \frac{\iiint \left(M(\delta s_j)\right)(D-d_{j-1}) d\boldsymbol{x_r}\, d\boldsymbol{x_s}\, d\omega}{\sqrt{\iiint \left(M(\delta s_j)\right)^2 d\boldsymbol{x_r}\, d\boldsymbol{x_s}\, d\omega \iiint (D-d_{j-1})^2 d\boldsymbol{x_r}\, d\boldsymbol{x_s}\, d\omega}}$.
7. Conduct regularization. Initialize $l_0 = r_{j-1} + \epsilon \delta s_j$, $q_0 = 0$, $b_0 = 0$ and conduct:
   a. For $i = 1,2,3,\ldots$ repeat steps b-d and exit with $r_j = l_i$ if stopping criterion has been met:
   b. Update l_i, q_i and b_i using equation (9), (10) and (11), respectively.
8. Compute modeling (for the next iteration) $d_j = M(r_j)$.

Examples

In the first example, we perform LSWEM on the Sigsbee2b 2D synthetic dataset. The WEM ADCIG using the standard cross-correlation imaging condition in Figure 1a shows unbalanced illumination from the left sedimentary to the subsalt area. Using a deconvolution imaging condition in equation (3), the general improvement of illumination and resolution is achieved in the WEM ADCIG (Figure 1b). The deconvolution imaging condition thus yields a more desired initial estimate and better adjoint than the conventional cross-correlation imaging condition. On close inspection of Figure 1b there remains some undesired amplitude decay and wavelet distortion at far angles due to the limited acquisition aperture. As shown in Figure 1c, over the entire angle range, the LSWEM has not only balanced angle illumination, but also enhanced resolution by broadening the frequency and wavenumber content (Figures 1e, 1f and 1g). For rigorous analysis without the illumination interference from the salt, we show a normalized amplitude verses angle (AVA) analysis using WEM and LSWEM at a typical diffraction point (arrowed location). In Figure 1d, LSWEM is able to accurately extend the amplitude behavior of the WEM ADCIG.

We also applied the LSWEM to a wide-azimuth data from the North Sea. The migration/demigration model is tilted transversely isotropic (TTI). In the Figure 2a which is generated by stacking the WEM ADCIG gathers at a typical subline, the shallow sediment geology below the water bottom suffers from reduced resolution. In particular, at the highlighted locations indicated by the squares, the segment and

fault structures are not well imaged for interpretation. After applying the LSWEM, in the stacked image (Figure 2b), the termination of the segment section, the continuity of the structures and the resolution (as demonstrated by images in Figures 2c and 2d and the f-k spectrums in Figures 2e and 2f) is improved.

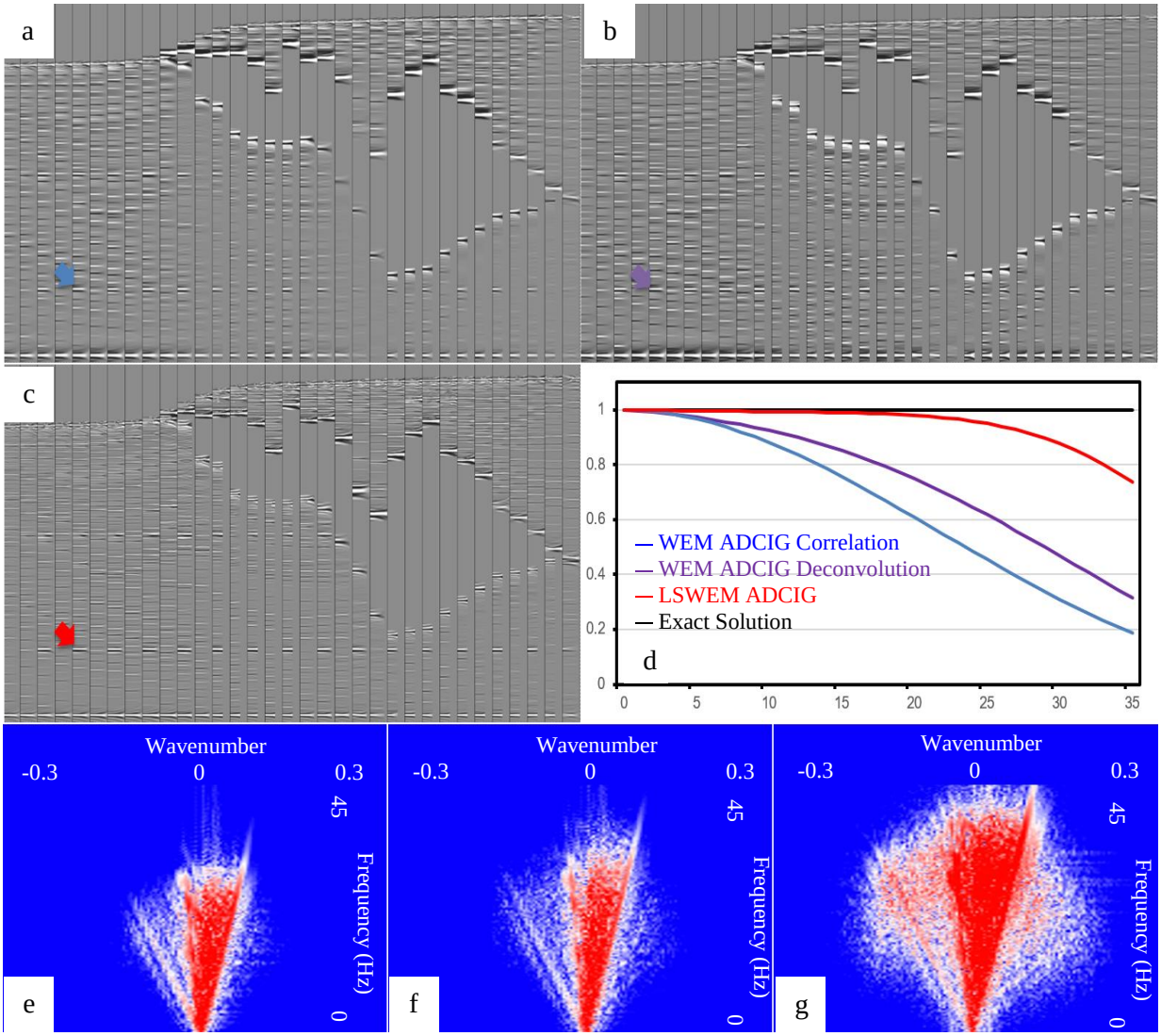

Figure 1: *Sigsbee2b 2D synthetic example: (a) WEM ADCIG with cross-correlation imaging condition; (b) WEM ADCIG with deconvolution imaging condition (3); (c) LSWEM ADCIG; (d) Normalized Amplitude Verse Angle analysis of a typical diffraction point at the arrowed location in (a), (b) and (c); (e) f-k spectrum of a typical angle volume for WEM ADCIG with cross-correlation imaging condition in (a); (f) f-k spectrum of the same angle volume in (e) for WEM ADCIG with deconvolution imaging condition in (b);(g) f-k spectrum of the same angle volume in (e) for LSWEM ADCIG in (c).*

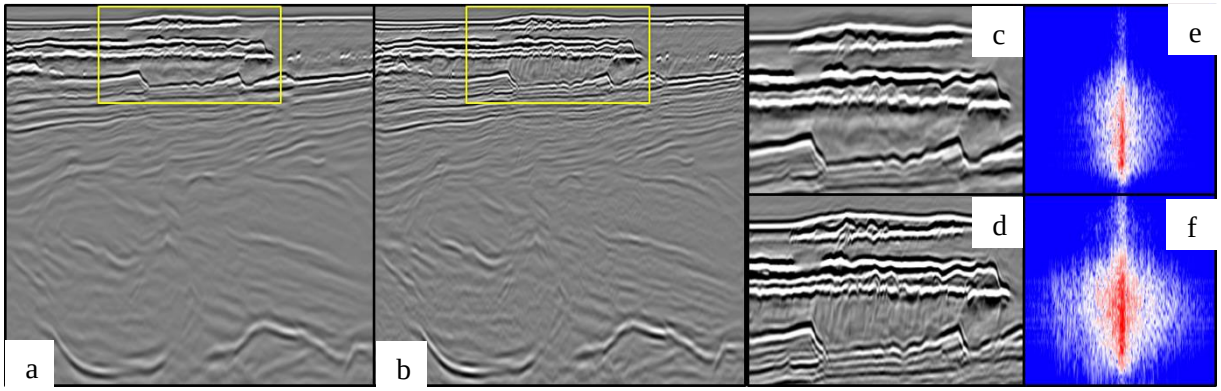

Figure 2 *North Sea 3D example: (a) stacked WEM image using ADCIG; (b) stacked LSWEM image using ADCIG; (c) zoom-in section of the highlighted area in (a); (d) zoom-in section of the highlighted area in (b); (e) f-k spectrum of the section in (c); (f) f-k spectrum of the section in (d).*

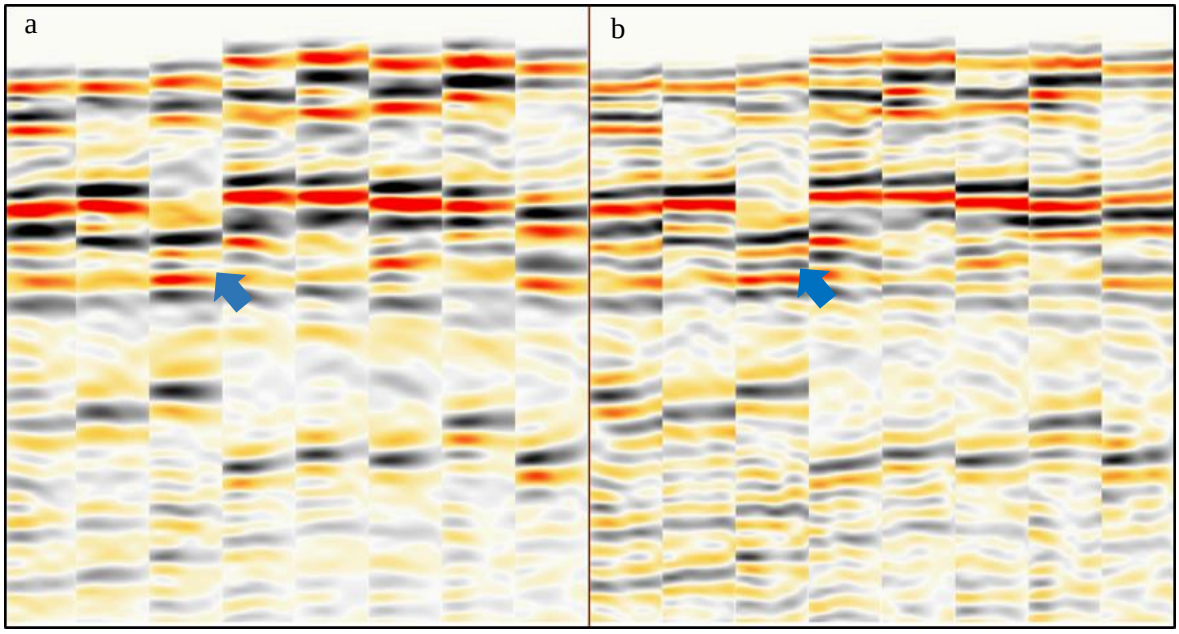

Figure 3 *North Sea 3D example: (a) WEM ADICG at evenly select crosslines for the section in Figure (2c); (b) LSWEM ADICG at evenly select crosslines for the section in Figure (2d).*

For detailed comparison, in the Figure 3, we present ADCIGs using WEM and LSWEM at the identical locations for the highlighted section. The same resolution and illumination improvement as observed in the stacked images (Figure 2) can be made in the subsurface angle domain. In particular, the LSWEM ADCIG achieves balanced amplitude from the near to the far angle demonstrating the improved AVA effect. The arrows in Figures 3a and 3b, show improvements in data resolution, which reduce tuning effects, resulting in more reliable amplitude behavior with angle. The angle domain results using LSWEM provide further validation and confidence for potential AVA analysis and interpretation.

Conclusions

Least-squares migration (LSM) for improving resolution and illumination and suppressing migration artifacts on stacked images is becoming a processing standard. Yet, its implementation and application in the prestack domain remains challenging. Using an extended demigration operator and deconvolution imaging condition, we have developed a prestack LSM framework in the extended subsurface domain. Both synthetic and field data experiments demonstrate that our proposed prestack LSM can improve the structural continuity, reveal weakly imaged details, extends the consistency in amplitudes over the subsurface angle range and improve angle domain amplitude balancing and illumination.

Acknowledgements

We thank PGS's Multi-Client Division for providing the datasets and our colleagues in PGS for their discussion and support, especially Øystein Korsmo, Tony Martin and Alejandro Valenciano.

References

Duan, L., Bekara, M., Baardman, R.H. and Lecocq, P. [2017] A practical method for multi-source deblending using spatio-temporal compressive sensing. *79th EAGE Conference and Exhibition*.

Fomel, S. [2011] Theory of 3-D angle gathers in wave-equation seismic imaging. *Journal of Petroleum Exploration and Production Technology*, **1**(1), 11-16.

Qiu L., Chemingui, N., Zou, Z., and Valenciano, A. A. [2016] Full-waveform inversion with steerable variation regularization. *86th Annual International Meeting*, SEG, Expanded Abstracts, 1174-1178.

Valenciano A. A., Chemingui N., Whitmore D., and Brandsberg-Dahl S. [2011] Wave equation migration with attenuation compensation. *73rd EAGE Conference & Exhibition.*

Lu, S., Liu, F., Chemingui, N., Valenciano, A., and Long, A. [2018] Least-squares full-wavefield migration. The Leading Edge, **37**(1), 46-51.